Boosting the Energy Efficiency of a Nanosecond Pulsed Corona Plasma System With a Multiple-Wire Plasma Reactor

T. Huiskamp, *Member, IEEE*, S. Subramanian, V. Gururajan, W. P. Schroeder, C. A. Schroeder, M. A. Gundersen, *Life Fellow, IEEE*, and S. B. Cronin

***Abstract*— Transient plasma generated by high-voltage nanosecond pulses in a pulsed corona configuration has proven to be an efficient medium for e.g., air purification applications. In this article, we present a study on boosting the energy efficiency of such a system by using a special type of plasma reactor: the multiple-wire plasma reactor. The basic principle of such a reactor is that it has a lower transmission-line impedance than a normal wire-cylinder reactor while at the same time still producing the required high electric fields necessary for plasma generation. The lower impedance of the reactor results in a smaller impedance mismatch between the high-voltage pulse source and the reactor, thereby minimizing pulse reflections on the source-reactor interface, increasing the energy efficiency of the system. We calculate the impedance of the multiple-wire reactor and assess both the electrical energy efficiency as well as the chemical efficiency of the plasma by measuring electrical energies and ozone concentrations generated by the plasma when energized by a fast solid-state nanosecond pulse source (with 7-ns rise time pulses of up to 20 kV) for a range of multiple-wire plasma reactor parameters. We show that with the multiple-wire reactor we can almost double the energy efficiency of the reactor (from 45% to 85%), reduce the voltage stress in the system by 29%–31% and increase the system efficiency by 95%–98% when using a multiple-wire electrode geometry (as compared to a single-wire system).**

***Index Terms*— Energy efficiency, high-voltage, pulsed power supply, transient plasma.**

I. Introduction

NON-THERMAL plasma can be generated efficiently with high-voltage pulses and is used for applications such as surface modification, air purification, and water decontamination [1]–[3]. The effectiveness of the plasma is based on the generation of reactive species, which can be produced very efficiently when short pulses are used. Furthermore, for large-volume plasma generation (necessary for industrial applications) the pulsed corona discharge is an ideal candidate [4]–[9]. This type of discharge typically consists of many parallel streamers which are generated by a high-voltage pulse on a wire electrode (normally, wire-cylinder or wire-plate plasma reactors are used for pulsed corona discharge generation). The duration of the high-voltage pulse is then made sufficiently short to prevent the discharge from developing into a full breakdown. In fact, it seems that the shorter the pulses are, the more efficient the reactive species can be generated [10]–[14].

In our project, we are looking into NO removal from diesel exhaust, a classical nonthermal plasma application. In this system, we use a nanosecond pulse source to generate a pulsed corona plasma. For this system to be commercially successful, it needs to be as energy-efficient as possible. Therefore, the main purpose of this study is to optimize the energy efficiency of the entire plasma system. Not only will this result in the best possible performance from the system as a whole, but it will also result in the least amount of high-voltage stress on all the system components. Combined, this will significantly enhance the efficiency, lifetime, and durability of the system.

Previous studies on plasma reactor efficiency found that increasing the E/n value in the plasma reactor (where E is the applied electric field and n is the gas density) increases the efficiency. For instance, increasing the applied voltage [15]–[22], decreasing the electrode distance [15], [16], [23], or imposing a dc-bias voltage [15], [17], [24], [25] all generally result in a higher electric field and therefore a higher dissipated energy in the plasma (and therefore result in a higher electrical efficiency). Likewise, when the gas density is decreased—either by lowering the pressure [26]–[29] or by increasing the temperature [26], [28]–[32]—the dissipated energy in the plasma increases. Additionally, the dissipated plasma energy also increases with a short rise time [19], [33] and long pulse duration (however, for long pulse durations the chemical efficiency of the plasma typically decreases if the pulse becomes so long that streamers can cross the electrode gap) [10], [19]. A thorough overview of plasma reactor efficiency as a function of different parameters is given in [19] and [34].

Manuscript received October 8, 2019; revised November 20, 2019; accepted November 23, 2019. This work was supported by Tai Chong Cheang Steamship Company (TCC). The review of this article was arranged by Senior Editor R. P. Joshi. *(Corresponding author: T. Huiskamp.)*

T. Huiskamp is with the Electrical Energy Systems Group, Department of Electrical Engineering, Eindhoven University of Technology, 5600 MB Eindhoven, The Netherlands (e-mail: t.huiskamp@tue.nl).

S. Subramanian, W. P. Schroeder, C. A. Schroeder, M. A. Gundersen, and S. B. Cronin are with the Ming Hsieh Department of Electrical and Computer Engineering-Electrophysics, University of Southern California, Los Angeles, CA 90007 USA.

V. Gururajan was with the Aerospace and Mechanical Engineering Department, University of Southern California, Los Angeles, CA 90007 USA. He is now with the Argonne National Lab, Lemont, IL 60439 USA.

Color versions of one or more of the figures in this article are available online at http://ieeexplore.ieee.org.

Digital Object Identifier 10.1109/TPS.2019.2956548

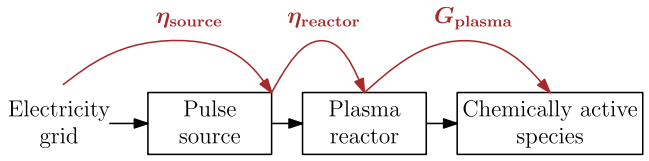

Fig. 1. Electrical energy from the electricity grid is formed into high-voltage pulses by the nanosecond pulse source. These pulses then generate plasma in the plasma reactor, where the electrical energy is converted into chemical energy. Each of these steps is performed with an associated efficiency. It is important to optimize each of these efficiencies to obtain the most efficient overall system.

The main method that we will use to boost the efficiency in our system (besides using a fast nanosecond pulse source) is the use of a multiple-wire plasma reactor. It was first proposed in [19], and we will use it for the first time in a study over a large number of parameters. By employing such a design, we ensure that the transmission-line impedance of the reactor is lower than a conventional reactor (resulting in a larger part of the pulse being transmitted into the plasma reactor) while still maintaining a high value of the electric field in the reactor, which is necessary for plasma development.

In this article, we will first discuss the important chain of efficiencies in the system in Section II, followed by a detailed analysis of the benefits and impedance of a multiple-wire reactor in Section III. Section IV will then describe the experimental setup and Section V will present the results, followed by the conclusions.

II. Efficiencies in the System

Fig. 1 shows an overview of the efficiencies that are important in the nanosecond pulsed corona plasma system.

Three efficiencies are important in the system:

1) *Source Efficiency:* Energy is taken from the electricity grid by the pulse source and converted into short pulses. The electrical efficiency with which it does this is η_{source}.
2) *Plasma Reactor Efficiency:* When the pulses are applied to the plasma reactor, plasma is generated. However, only part of the energy from the pulses is dissipated by the plasma. The electrical efficiency of the plasma reactor $\eta_{reactor}$ is therefore defined by

$$\eta_{reactor} = \frac{E_{plasma}}{E_{pulse}} \tag{1}$$

   where E_{plasma} is the energy that is dissipated by the plasma (in J) and E_{pulse} is the total available energy per pulse (in J).
3) *Chemical Efficiency:* Finally, the energy that is used by the plasma, is converted into chemically active species. The efficiency with which the plasma performs this conversion is called the chemical plasma efficiency G_{plasma}. A detailed definition of this parameter will be given in Section IV.

The total system efficiency is the product of all three efficiencies (i.e., in every step, energy is lost). Since the source efficiency is not under our control (it was developed by a third party), the main purpose of this investigation is to maximize the total plasma reactor system efficiency ($\eta_{reactor} \times G_{plasma}$).

A. Plasma Reactor Efficiency

The electrical efficiency of the reactor is influenced by two parameters: the electric field strength at the high-voltage wire in the reactor and the impedance-matching of the reactor.

The electric field strength in the reactor is determined by the geometry of the reactor. For a standard wire-cylinder reactor it holds that the thinner the high-voltage wire and the closer the wire is to the grounded cylinder, the higher the electric field. The electric field strength needs to be high for pulsed corona plasma to be generated with any intensity, resulting in the efficient use of electrical energy.

The impedance-matching of the system determines how much of the pulse enters the plasma reactor, because whenever an electromagnetic wave encounters a change in impedance, it will partly reflect and partly transmit. Since most plasma reactors have a different impedance than the output impedance of a pulse source, in reality, there will always be some reflection. This reflection and transmission can be calculated with the reflection coefficient R and the transmission coefficient T

$$R = \frac{Z_{reactor} - Z_{source}}{Z_{reactor} + Z_{source}} \tag{2}$$

$$T = \frac{2Z_{reactor}}{Z_{reactor} + Z_{source}} \tag{3}$$

where Z_{source} is the impedance of the pulse source (or the cable that connects the pulse source to the plasma reactor) and $Z_{reactor}$ is the transmission-line impedance of the plasma reactor, which for a wire-cylinder reactor is given by

$$Z_{reactor} = \frac{1}{2\pi}\sqrt{\frac{\mu_0}{\epsilon_0}}\ln\frac{d_o}{d_i} \tag{4}$$

where μ_0 and ϵ_0 are the permeability and permittivity of vacuum, respectively, d_o is the inner diameter of the outer conductor of the reactor and d_i is the diameter of the wire electrode of the reactor. Here, we assume that the reactor is a perfect coaxial structure. Furthermore, (4) neglects the influence of the plasma on the reactor impedance. In reality, the impedance will decrease as the plasma develops, which makes the reflection and transmission coefficient time-dependent [19].

For a perfectly matched system, the entire pulse enters the plasma reactor, which is the ideal situation. However, when there is a mismatch, the pulse partly reflects off the plasma reactor. This leads to the following.

1) *Loss of Energy:* The part of the pulse that does not enter the reactor is partly lost when it travels back to the pulse source.
2) *Increased High Voltage Stress in the System:* For the fast pulses we use in this article, the reflected pulse adds to the incoming pulse, increasing the voltage in the system at some parts. Increased high-voltage stress may lead to increased aging of system components or even to failure of the system due to high-voltage breakdown.

For a standard wire-cylinder reactor $Z_{reactor}$ is around 250–300 Ω. Since the impedance of the typical pulse source

system is lower than this (50 Ω in our case), such a standard solution is significantly mismatched, resulting in energy loss and increased high-voltage stress in the system. A solution to this problem is to use a multiple-wire electrode, which will significantly decrease the impedance of the reactor and thereby increase energy efficiency. This design was first proposed in [19] (where the first results showed an increase in η_{reactor} of almost 20%) and will be further explored here. This type of reactor will be described in detail in Section III.

B. Chemical Efficiency

The chemical efficiency of the plasma reactor (how much chemically active species are formed as a function of the dissipated energy in the plasma) is difficult to determine directly since chemically active species are short-lived (typically less than 100 μs) and complicated and expensive investigative techniques would be required to quantify such species. An exception is the ozone, which is a long-lived radical species and can be used as a marker to estimate how efficiently plasma forms all chemically active oxygen species. The quantity with which this is measured is the ozone yield in g·kWh^{-1}. This quantity is often used by the international community as a measure for plasma efficiency. Therefore, in this article, the ozone yield is used as a measure for chemical efficiency of our corona plasma. Section IV explains how this yield was calculated. Here, we should mention that this plasma efficiency is defined as the efficiency with which the plasma converts energy into ozone in our system and at room temperature.

III. Multiple-Wire Plasma Reactor

In this section, we explore the concept and impedance-analysis of the multiple-wire reactor.

A. Concept

When using a regular wire-cylinder reactor (i.e., with only one central wire) a small wire diameter in the reactor intuitively increases the reactor efficiency (increase $\eta_{reactor}$) because of the higher electric field a small wire diameter generates (as opposed to a large wire diameter). However, a smaller wire diameter will also increase the reflection coefficient—calculated with (2)—and therefore more energy is reflected at the source–reactor interface, which decreases the reactor efficiency. Therefore, it seems likely that there is some optimum wire diameter for wire-cylinder pulsed corona reactors. This analysis was confirmed by experiments in [19], though the effect when using wire diameters in the range of 0.3–1 mm in a 50-mm diameter plasma reactor was not too significant and an optimum was found in the middle of the range of wire diameters. In other words, when using a single wire, the optimum wire diameter from a reactor-efficiency point of view results in quite a high impedance of the plasma reactor.

The best way to transmit the largest part of the incoming pulse into the reactor is by increasing the wire diameter substantially. However, to be still able to ignite a discharge, the electric field at the wire has to be high enough, which is a condition that is not satisfied with a large conductor. This problem is solved with the multiple-wire plasma reactor.

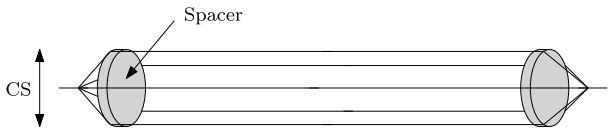

Fig. 2. Example of a multiple-wire electrode for a plasma reactor. This multiple-wire configuration replaces the single wire that is normally used in a wire-cylinder plasma reactor.

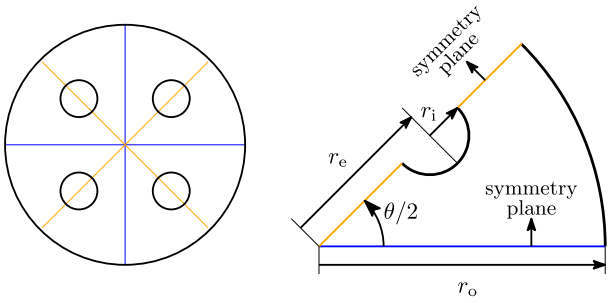

Fig. 3. Left: example of a cross-sectional view of a 4-wire multiple-wire electrode system used for the calculation. Right: symmetrical slice used for the simulations.

Fig. 2 shows an example of a multiple-wire configuration. A number of wires N_w (=5 in the example) are mounted in such a way that they are positioned away from the center of the reactor. This is achieved by the use of two plastic spacers that keep the wires in place at equal distance from each other at a certain cross section, CS. The multiple-wire assembly is then tightened into place in the reactor (more details will be shown in Section IV).

With the multiple-wire conductor the electric field close to the wires will be high but perhaps not as high as with a single-wire conductor, since the proximity of the other wires will partly screen the electric field. However, the electric field is high enough for plasma to be able to ignite on the wires and the close proximity to the grounded cylinder also increases the electric field. A downside of the multiple-wire configuration is that the plasma is not as homogeneous as with a single-wire configuration as was already shown in [19], though this did not seem to affect the plasma efficiency.

B. Impedance Calculations

For a calculation of the impedance of a reactor geometry, we usually prefer analytical solutions, like (4). However, neat analytic solutions exist only for a handful of geometries; the general problem requires recourse to numerical methods. Luckily, Kaden [35] calculated the capacitance and inductance of a great number of uncommon geometries, including our geometry of the multiple-wire electrode system. For the calculation, we refer to Fig. 3. Here, we define r_o and r_i as the radius of the outer grounded cylinder and the radius of the individual wires, respectively. Furthermore, r_e is the distance from the center of a wire to the center of the system. We further define

the nondimensional variable p as

$$p = \frac{N_{\mathrm{w}}}{2} \tag{5}$$

where N_{w} is the number of wires used in the multiple-wire inner electrode of the reactor.

Kaden gives the solution for the capacitance per unit length C' (in F/m) as

$$C' = \frac{4p\pi\epsilon_{\mathrm{r}}\epsilon_0}{\ln\frac{r_{\mathrm{o}}^{4p}-r_{\mathrm{e}}^{4p}}{2pr_{\mathrm{e}}^{2p-1}r_{\mathrm{o}}^{2p}r_{\mathrm{i}}} - \left[2p-1+\frac{4pr_{\mathrm{e}}^{4p}}{r_{\mathrm{o}}^{4p}-r_{\mathrm{e}}^{4p}}\right]\left(\frac{r_{\mathrm{i}}}{2r_{\mathrm{e}}}\right)^2}. \tag{6}$$

Given the definition (in a coaxial structure)

$$\frac{1}{\sqrt{L'C'}} = c \tag{7}$$

where c is the speed of light in vacuum and L' (in H/m) the inductance per unit length, we can calculate the impedance of the multiple-wire reactor with

$$Z = \sqrt{\frac{L'}{C'}} = \frac{1}{cC'}. \tag{8}$$

Unfortunately, Kaden only specifies the analytical solution for $p=1$ and 2, i.e., for a 2-wire and 4-wire electrode, respectively. Since we want to be flexible in the number of wires we use, we performed numerical calculations to verify if we can use (6) for an arbitrary number of wires. Here, we use the finite volume method, utilizing the numerical tensor calculus suite OpenFOAM [36], in particular, a Laplacian solver. Mesh independent solutions (i.e., solutions varying by less than 1% upon doubling the number of grid points) were arrived at by using a series of grids (corresponding to the geometry shown in Fig. 3) with finer mesh spacing near the highly curved regions. The total number of grid points did not exceed 80 000.

The electric potential ϕ in the vicinity of conductors, in the absence of other charges, is given by the solution to Laplace's equation with Dirichlet boundary conditions imposed on the surfaces of the conductors as they are equipotential surfaces [37]

$$\nabla^2\phi = 0. \tag{9}$$

Once Laplace's equation is solved, the gradient of the electric potential normal to a conductor's surface $\partial\phi/\partial n$ (which is just the electric $\vec{E}$ field at the surface) at a point $\vec{r}$ on the surface, is related to the surface charge density, σ via

$$\frac{\partial\phi}{\partial n}\hat{n}(\vec{r}) = \vec{E}(\vec{r}) = \frac{\sigma(\vec{r})}{\epsilon_0}. \tag{10}$$

The total charge Q on the surface S is then just

$$Q = \oint_S \frac{\partial\phi}{\partial n}\hat{n}(\vec{r})dS. \tag{11}$$

The capacitance of a system of conductors involving two different potentials can then be calculated by

$$C = \left|\frac{Q}{\phi_2 - \phi_1}\right| \tag{12}$$

where ϕ_2 and ϕ_1 are the two different potentials.

Three new variables are introduced, which are used in the calculations

$$\alpha = \frac{r_o}{r_e} \tag{13}$$

$$\beta = \frac{r_o}{r_i} \tag{14}$$

$$\theta = \frac{2\pi}{N_{\mathrm{w}}}. \tag{15}$$

The results of both the numerical calculations as well as calculations using Kaden for a range of α, β, and N_{w} values are shown in Fig. 4. From the results we can conclude that for the range of values that we performed these calculations, the formula of Kaden may also be used for values other than $p=1$ and 2. Other observations from the results are relatively obvious, such that the impedance is higher (lower C') for less wires and thinner wires, as well as for a shorter distance between the wires and the center of the reactor.

IV. Experimental Setup and Diagnostics

A diagram of the total experimental setup that we used is shown in Fig. 5. Each part will be explained in more detail in the next sections.

A. Pulse Source

The pulse source that was used in this article was a SSPG-20X-HP1 pulse generator from Transient Plasma Systems, Inc. [38]. It is a high-repetition rate (up to 20 kHz), solid-state pulse source with an adjustable output voltage of up to 20 kV, a FWHM pulse duration of around 12–15 ns and a 10%–90% rise time of around 7 ns. The pulse source is connected to the plasma reactor with a 2-m long 50-Ω cable. Fig. 6 shows an example waveform on a 50-Ω matched load.

B. Plasma Reactor and Electrode Configurations

Fig. 7 shows the plasma reactor system that we used. It is a system that was previously used at USC with actual diesel exhaust and is therefore rated for high temperatures (up to 260 °C). The system comprises several sections. First, a measurement section with a D-dot and B-dot sensor for electrical measurements (see Section IV-C). Second, a high-temperature section that maintains the 50-Ω impedance of the system (and therefore minimizes pulse reflections) and features a gas inlet (only a small diameter for our measurements but a large diameter exhaust pipe can be connected as well). Third, the plasma reactor, which is a 0.91-m (3-ft) long tube with an inner diameter of around 55 mm (2.16 in). A wire, or multiple-wire electrode assembly can be tightened at the center of the reactor as a high-voltage electrode. The final section is a T-section with the gas exhaust, a window and the tightening mechanism for the high-voltage electrode.

Fig. 8 shows the electrodes we used. Besides the "normal" configuration of a single wire that almost all researchers use, we used multiple-wire electrodes (up to six wires per electrode) and finally two extruded electrodes. These extruded electrodes are solid metal along their length, with four sharp edges each. The reasoning behind using these electrodes is that

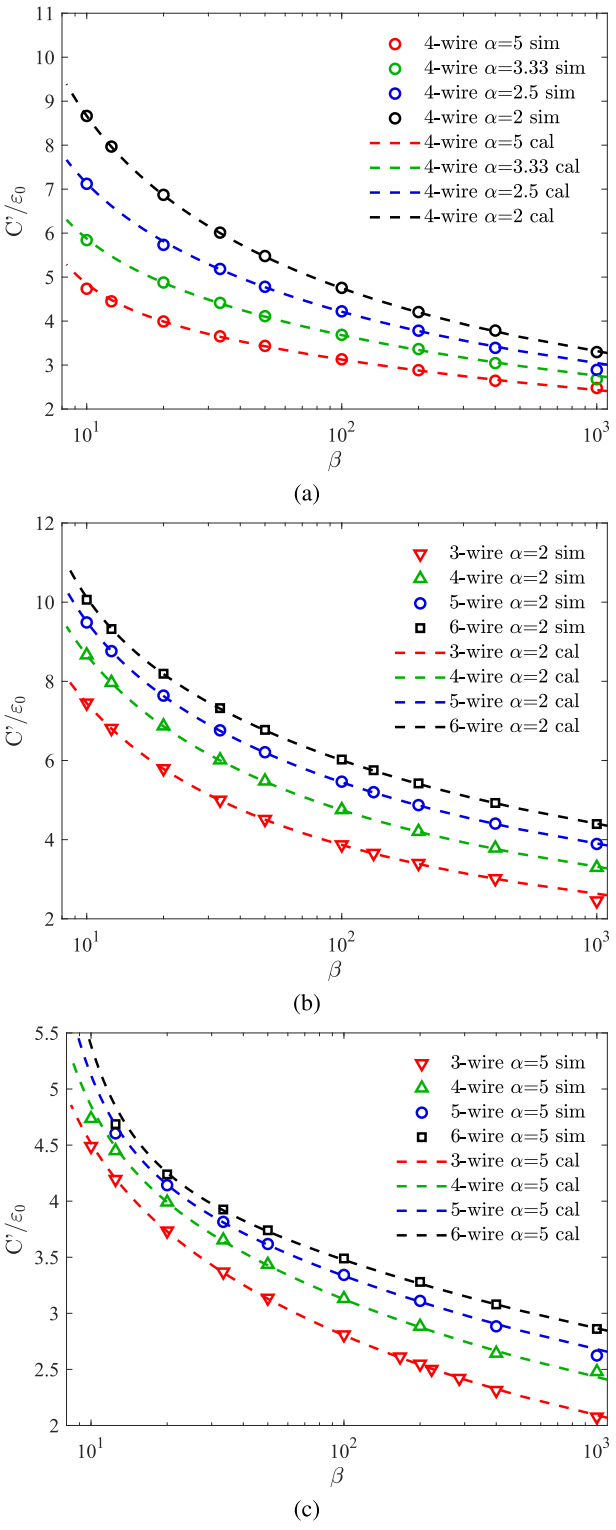

Fig. 4. Capacitance per unit length for a range of α, β, and N_w values. The points denoted with "sim" are from the numerical calculation, whereas the dashed lines are calculated with (6). (a) α and β are changed for a 4-wire electrode. (b) and (c) β and the number of wires are changed for $\alpha = 2$ and $\alpha = 5$, respectively.

they will potentially work as well as the 4-wire electrodes, but are much more sturdy and robust, which can be an advantage in real applications. Fig. 9 shows an example of the appearance of the discharge with the 4-wire electrode.

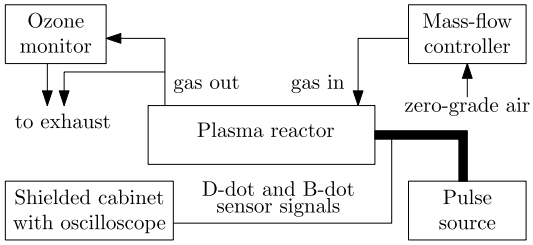

Fig. 5. Block diagram of the experimental setup. On the electrical side, a nanosecond pulse source delivers pulses to a plasma reactor, generating a pulsed corona plasma. The voltage and current in the system are measured with D-dot and B-dot sensors, which connect to an oscilloscope in a shielded cabinet. On the gas side, zero-grade air (ZGA) is fed into the plasma reactor with a mass-flow controller. At the exhaust of the plasma reactor, we measure the ozone concentration with an ozone monitor.

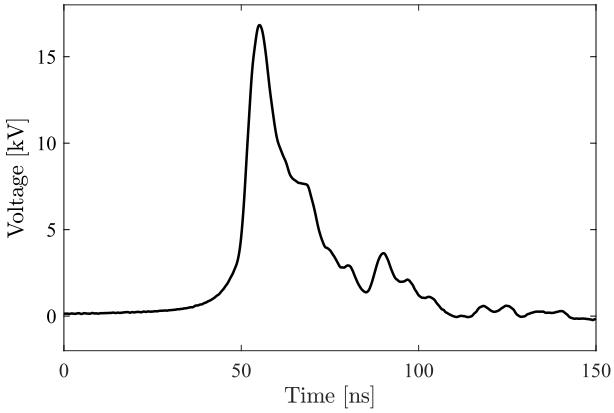

Fig. 6. Example waveform from the SSPG-20X pulse source on a matched 50-Ω load.

Table I lists all the electrodes we used, together with their calculated impedances (according to the calculations from Section III). We used three wire diameters: 15, 25, and 40 mil (0.381, 0.635, and 1.016 mm, respectively). This corresponds to $\beta = 144$, 86.4, and 54, respectively (with a 2.16-in reactor diameter). Additionally, we used four cross sections for the multiple-wire electrodes: 0.43, 0.65, 0.86, and 1.08 in (10.9, 16.5, 21.8, and 27.4 mm, respectively). This corresponds to $\alpha = 5$, 3.3, 2.5, and 2, respectively (and therefore to some of the traces in Fig. 4). Each wire assembly is made to the same length of 36 in (91.4 cm).

C. Electrical Diagnostics

The voltage and current in the plasma system are measured with D-dot and B-dot sensors [39], [40]. These sensors are installed in the cable connector (see Fig. 7) and measure the derivative of the displacement field and magnetic field intensity associated with the voltage and current, respectively. The D-dot sensor is an electrode soldered to an SMA connector and pointed at the high-voltage electrode. The B-dot sensor is made in a similar fashion, only now the electrode forms a loop and is also soldered onto the grounded measurement box to close the circuit.

The sensor signals are measured with an oscilloscope (1-GHz Bandwidth, DPO5104 Tektronix) placed in a shielded cabinet for disturbance-free measurements. Passive integrators mounted on the oscilloscope integrate the measured

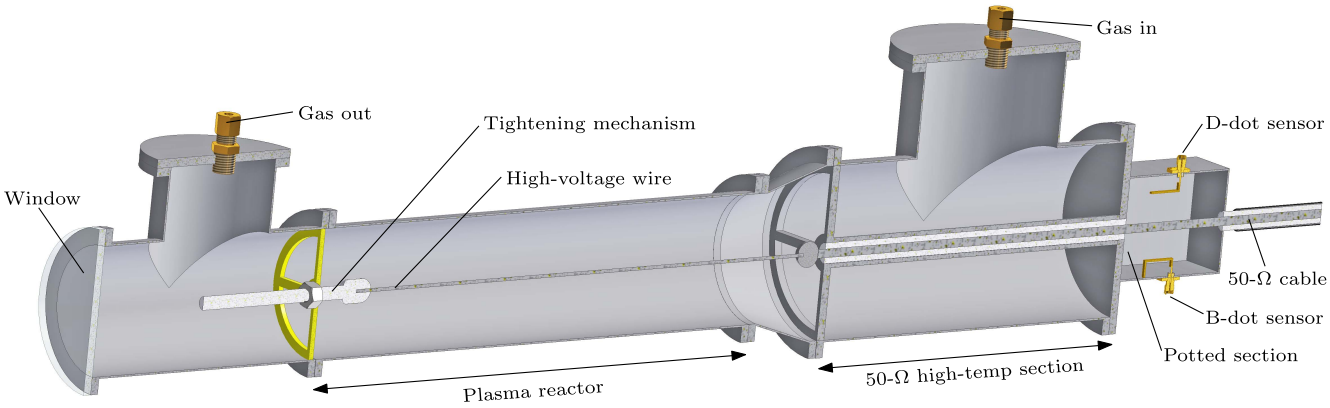

Fig. 7. Sketch of the plasma reactor system. From right to left, a 50-Ω cable that connects to the pulse source enters an epoxy-potted section (epoxy not shown in the figure). A D-dot and B-dot sensor is mounted in this section for voltage and current measurements, respectively. This measurement section is followed by a high-temperature section, a section that has a 50-Ω impedance (the pulse travels through the inner coaxial structure) and can withstand high temperatures. It is followed by the plasma reactor (not drawn to scale; it is longer in reality) which is just over 0.91 m long (3 ft) and has an inner diameter of just under 55 mm (2.16 in). A tightening mechanism holds the high-voltage wire (drawn thicker for clarity) taut and in the center of the plasma reactor. This single wire can be replaced by multiple-wire electrode assemblies (see Figs. 2 and 8). T-sections before and after the plasma reactor further have a gas inlet, gas outlet, and a window.

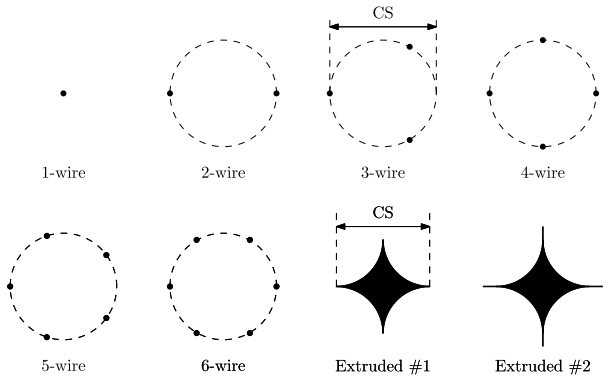

Fig. 8. Overview of the multiple-wire electrode assemblies that were used in this study. Note that the outer grounded cylinder is not shown. The figure shows the cross section of the electrodes (the dashed circles indicate the plastic spacers that were used, see Fig. 2). We also used the two extruded electrodes on the right. These are solid metals.

Fig. 9. Example of a pulsed corona plasma generated with a 4-wire electrode.

waveforms and thereby reconstruct the actual voltage and current waveforms. The main advantages of using these types of sensor are that the signal-to-noise ratio is excellent and that they are nonintrusive to the system (they have little to no impact on the high-voltage waveform). The disadvantage of the sensors is that low-frequency components of the signal cannot be measured and that waveform reconstruction and calibration have to be carefully done. However, the pulses to be measured have no significant low-frequency content and the waveform reconstruction and calibration can be done with little error. Therefore, the advantages far outweigh the disadvantages. A more detailed description of this type of sensor system can be found in [41, Ch. 2].

TABLE I

USED ELECTRODE GEOMETRIES AND THEIR CALCULATED IMPEDANCE (HERE N_W IS THE NUMBER OF WIRES IN THE GEOMETRY)

N_W	Wire diameter	Cross-section	α	β	$Z_{calculated}$
1	15 mil				298 Ω
1	25 mil				267 Ω
2	15 mil	0.86”	144	2.5	155 Ω
2	15 mil	1.08”	144	2.0	147 Ω
2	25 mil	0.86”	86.4	2.5	140 Ω
3	15 mil	0.65”	144	3.3	125 Ω
3	15 mil	0.86”	144	2.5	114 Ω
3	15 mil	1.08”	144	2.0	105 Ω
3	25 mil	0.86”	86.4	2.5	104 Ω
4	15 mil	0.86”	144	2.5	95.0 Ω
4	15 mil	1.08”	144	2.0	84.8 Ω
4	25 mil	0.43”	86.4	5.0	118 Ω
4	25 mil	0.65”	86.4	3.3	99.9 Ω
4	25 mil	0.86”	86.4	2.5	87.4 Ω
4	25 mil	1.08”	86.4	2.0	77.1 Ω
4	40 mil	0.86”	54.0	2.5	80.3 Ω
5	15 mil	0.86”	144	2.5	84.4 Ω
5	15 mil	1.08”	144	2.0	73.5 Ω
5	25 mil	0.86”	86.4	2.5	78.3 Ω
6	15 mil	0.86”	144	2.5	77.7 Ω
6	15 mil	1.08”	144	2.0	66.3 Ω
6	25 mil	0.86”	86.4	2.5	72.6 Ω
	Extruded	0.80”			
	Extruded	1.08”			

The power and energy are calculated from the D-dot and B-dot sensors with

$$P(t) = I_B(t)V_D(t) \tag{16}$$

$$E(t) = \int_0^t P(\tau)\,d\tau. \tag{17}$$

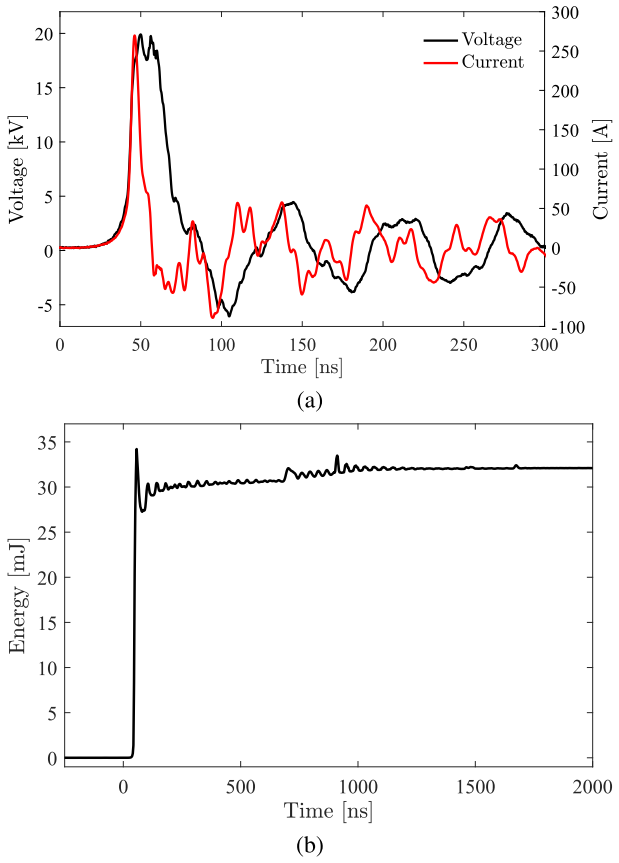

Fig. 10. Example waveforms in the plasma system. (a) Voltage and current. (b) Energy experimental settings were: 16-kV applied voltage, 4-wire electrode with 15-mil diameter wire and 0.86" cross section. Note that the measured voltage is higher than the applied voltage due to a reflection on the reactor interface.

Fig. 10 shows example measurements when plasma is generated in the reactor. Since the plasma reactor is not a matched load, reflections occur which increases the apparent duration of the pulse (compare to Fig. 6). Additionally, from the energy waveform, we can see that not all energy is dissipated during the initial pulse. Also the reflections still add energy to the plasma. The extra bump in energy at around 700 ns is due to the pulse source generating a small pulse again at this time, which adds a little more energy to the plasma. The end value of the energy waveform (i.e., the energy at around 2000 ns) is used for the calculation of the ozone yield (see Section IV-E) and the calculation of reactor efficiency (see (1)). The value of E_{pulse} in the reactor efficiency calculation is the maximum value of energy that the pulse source delivers per pulse (at a specified voltage setting). We calculated this value from energy measurements on a matched load for a range of voltage settings.

D. Gas Delivery System

A mass flow controller (Cole-Parmer Model MC-50 SLPM-D) was employed to deliver a precise flow of ZGA to the plasma reactor. As the nature of these experiments requires the consumption of a significant volume of air, a ZGA generator system was built to circumvent the economic and time constraints of frequent ZGA cylinder replacement. This comprised a standard air compressor fit with a series of filtering components to remove moisture, particulates (down to 0.003 μm), and residual oil vapor.

E. Ozone Diagnostics

We measured the ozone concentration with a Teledyne Model 465L ozone analyzer, which can measure ozone concentrations up to 500 ppm.

The ozone yield (in g·kWh^{-1}) is now our plasma efficiency G_{plasma} (for this study, in our system and at room temperature) and can be calculated with

$$G_{\text{plasma}} = \frac{C_{O_3} \times 48 \times 3.6}{V_{\text{m}} \varepsilon} \tag{18}$$

where C_{O_3} is the measured ozone concentration (in ppm), V_{m} is the molar volume (24.5 L·mole^{-1} at room temperature), and ε is the energy density (in J·L^{-1}), which is given by

$$\varepsilon = \frac{f_{\text{rr}} E_{\text{p}} \times 60}{F} \tag{19}$$

where f_{rr} is the repetition rate of the pulse source, E_{p} is the total dissipated energy per pulse by the plasma (in J) and F is the gas flow (in L·min^{-1}) [19].

Since it is our goal to optimize the total efficiency of the pulsed corona plasma system, we also calculate the system efficiency, which is given by $\eta_{\text{reactor}} \times G_{\text{plasma}}$.

F. Measurement Uncertainty Analysis

Here, we briefly analyze measurement uncertainty (presented in the list below). We differentiate between system uncertainty (a fixed uncertainty introduced by the measurement system) and a statistical uncertainty (introduced by the statistical nature of the plasma and the random noise of the oscilloscope).

1) *Voltage and Current:* The uncertainty on the voltage and current measurements are roughly 5% system uncertainty and 2% statistical uncertainty. The statistical uncertainty is mostly eliminated by averaging over multiple waveforms.
2) *Ozone Concentration:* The uncertainty on the ozone concentration is mainly system uncertainty and is about 2%. All experiments were performed twice and the results averaged. Experiments were performed once from a low voltage to high voltage and vice versa for the second experiment to eliminate any settling issues with the ozone concentrations.
3) *Reactor Efficiency:* System uncertainty from the energy measurement (introduced by the voltage and current measurement) is mostly canceled because it is the same for both the dissipated energy as well as the calibrated maximum energy. However, new system uncertainty is introduced by the mounting of the wire electrodes and slight manufacturing offsets. Each experiment was performed twice, unmounting and mounting the electrodes between the runs to minimize this effect. The total uncertainty on the reactor efficiency is estimated to be 5%–7.5%.

4) *Ozone Yield:* All quantities come into play here. The total uncertainty on the ozone yield is estimated to be at around 10%.
5) *Total System Efficiency:* The uncertainty on the total system efficiency is estimated to be around 10%–12%.

V. Experimental Results and Discussion

In this results section, we focus on the reactor efficiency and voltage stress in the system over a wide range of reactor parameters. Here, we note that we did not use error bars in the figures in this section for better readability. However, a full uncertainty analysis was provided in the previous section.

A. Effect of the Voltage Amplitude

Fig. 11 shows the reactor efficiency, ozone yield, and system efficiency as a function of the pulse voltage and the number of wires used in the multiple-wire electrode assembly. The first observation is that reactor efficiency increases with the applied voltage. Since the reduced electric field (E/n) increases with the applied voltage, it is expected that the dissipated energy in the plasma increases (increasing the reactor efficiency), as we already stated in the introduction. At the same time, the ozone yield also increases with the voltage (for the 0.86-in cross section wire configuration), indicating that as long as the electric field increases, ozone can be generated more efficiently. However, for the 1.08-in cross section, the ozone yield actually decreases with the voltage. It is likely that at these settings the energy dissipated by the plasma is such that the energy density of the plasma becomes high enough to destruct ozone because the higher energy density results in an increase in gas temperature (the temperature of the neutrals in the gas) and an increase in the concentration of NO_x. Both of these effects promote the reaction of ozone with NO_x and consequently reduce the ozone concentration [42]–[44]. This energy density for the large cross sections is further enhanced due to the shorter distance from the wires to the wall, because when the discharge is formed over a shorter distance—while also dissipating more energy—the local energy density in the discharge is even higher (resulting in an even higher gas temperature). However, even though the ozone yield decreases with the voltage for the 1.08-in cross section electrodes, the system efficiency remains relatively constant with the voltage (due to the increased reactor efficiency at the higher voltages).

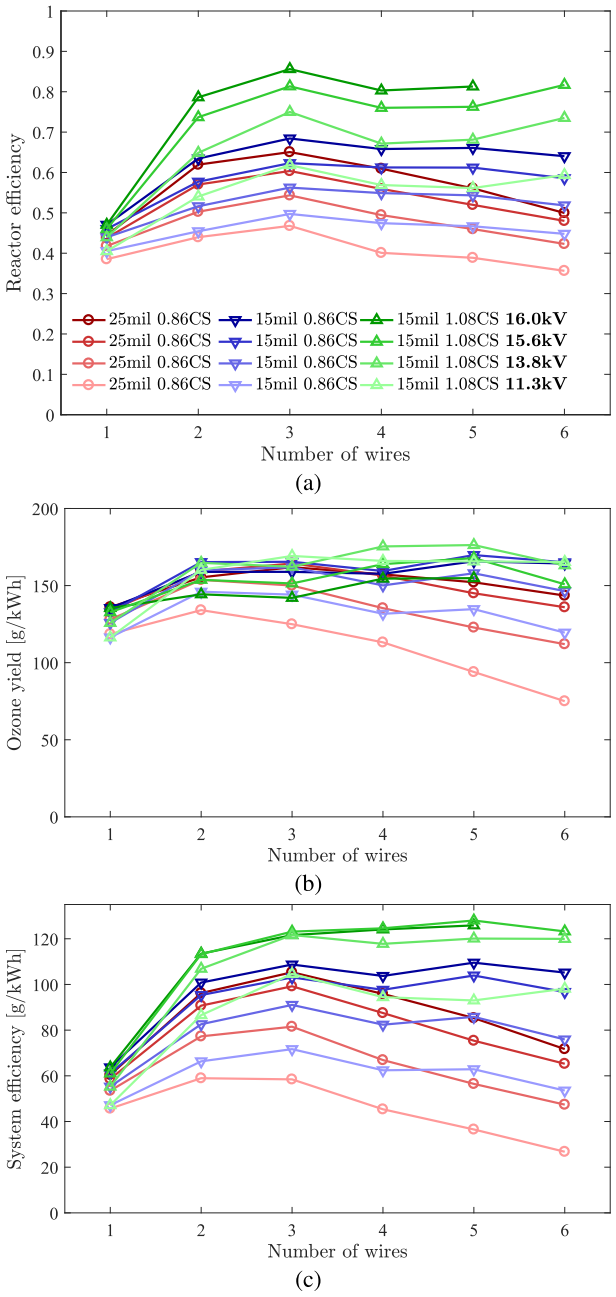

Fig. 11. (a) Reactor efficiency, (b) ozone yield, and (c) system efficiency as a function of the pulse voltage and the number of wires used in the multiple-wire electrode assembly (for several configurations). The gas flow was 5 slm and the pulse repetition rate 50 Hz.

B. Effect of the Number of Wires

Besides optimizing energy efficiency in the system, minimizing impedance mismatch between the reactor and the pulse source system serves another important purpose: minimization of voltage stress in the system. We will first discuss and analyze this voltage stress before commenting further on the results of Fig. 11.

As described before, when the reactor system is mismatched the high-voltage pulse will reflect off the reactor interface. It prevents energy from entering the plasma reactor, but the reflected pulse will also add to the incoming pulse, increasing the voltage in the system locally. How much the voltage is increased, is determined by the reflection coefficient R, which was given by (2).

For a perfectly matched system ($Z_{\text{reactor}} = Z_{\text{cable}}$), the reflection coefficient is 0 and no pulse reflection occurs. However, if the reactor impedance is 100 Ω (a realistic value, see Table I), for instance, then R is $\frac{1}{3}$. The maximum voltage stress $V_{\max}$ in the system is the addition of the reflected pulse and the incoming pulse, which is roughly

$$V_{\max} \approx (1 + R)V_{\text{peak}} \tag{20}$$

where V_{peak} is the applied peak voltage. So for the example, a voltage of 1.33 times the peak voltage is the maximum voltage stress in the system. It is important to minimize this, because any increased voltage stress potentially decreases the lifetime and reliability of the system.

In reality, the impedance of the plasma reactor is not constant; it starts off at the calculated reactor impedance (see Table I), but drops as soon as plasma develops. Fig. 12 shows what happens in the real system for different wire geometries. It shows the voltage measured at the D-dot sensor position for the same experimental settings as in Fig. 11.

Starting with Fig. 12(a), we observe an interesting effect: the first reflection (marked in the figure) decreases with the number of wires. This is exactly the effect described above: when the reactor impedance drops (which drops with the number of wires, see Table I), the voltage stress in the system decreases at that point in time. However, the part of the pulse that is transmitted into the plasma reactor has to generate a streamer plasma. If the energy in the pulse is not sufficiently dissipated by the plasma, the pulse then reflects off the end of the reactor (the side farthest from the pulse source) and then transmits back to the pulse source, where it also adds to the voltage at the reactor interface (where the sensor is located) and increases voltage stress as well. This is the second reflection, as marked in the figure. So the conclusion from Fig. 12(a) is that while the lower reactor impedance with an increased number of wires clearly decreases the reflected pulse amplitude, it also decreases the energy that is dissipated in the plasma, thereby increasing the voltage stress at a later stage of the pulse. Likewise, since less energy is dissipated in that situation, the reactor efficiency is also lower for large number of wires (see Fig. 11(a)). An optimum is found at around three wires for the reactor efficiency and for the system efficiency there are no significant differences in the range of 3–6 wires.

C. Effect of the Wire Diameter

When the wire diameter is decreased to 15 mil (see Fig. 12(b)), the second reflected pulse is much lower (where with the 25-mil wire the second reflection increased with N_{w}), because the thinner wire ensures a higher electric field at the wires, which in turn results in a higher plasma dissipation and therefore a lower reflected second pulse. Similarly, in Fig. 11 we already see that the 15-mil wire outperforms the 25-mil wire. Additionally, Fig. 13 shows results for a 4-wire electrode with a cross section of 0.86 in and wire diameters of 15, 25, and 40 mil. The corresponding impedances are 95.0, 87.4, and 80.3 Ω, respectively. So even though the impedance of the thinnest wire is the highest, the reactor efficiency is higher for this electrode. Again, the ozone yield clearly shows why: for thinner diameter wires the generated plasma generates more ozone, which indicates that the electric field was higher, which generates more efficient streamers. In other words, energy can be dissipated more efficiently for thinner wires (again, because the electric field is higher). Consequently, also the system efficiency is highest for the thinnest wire.

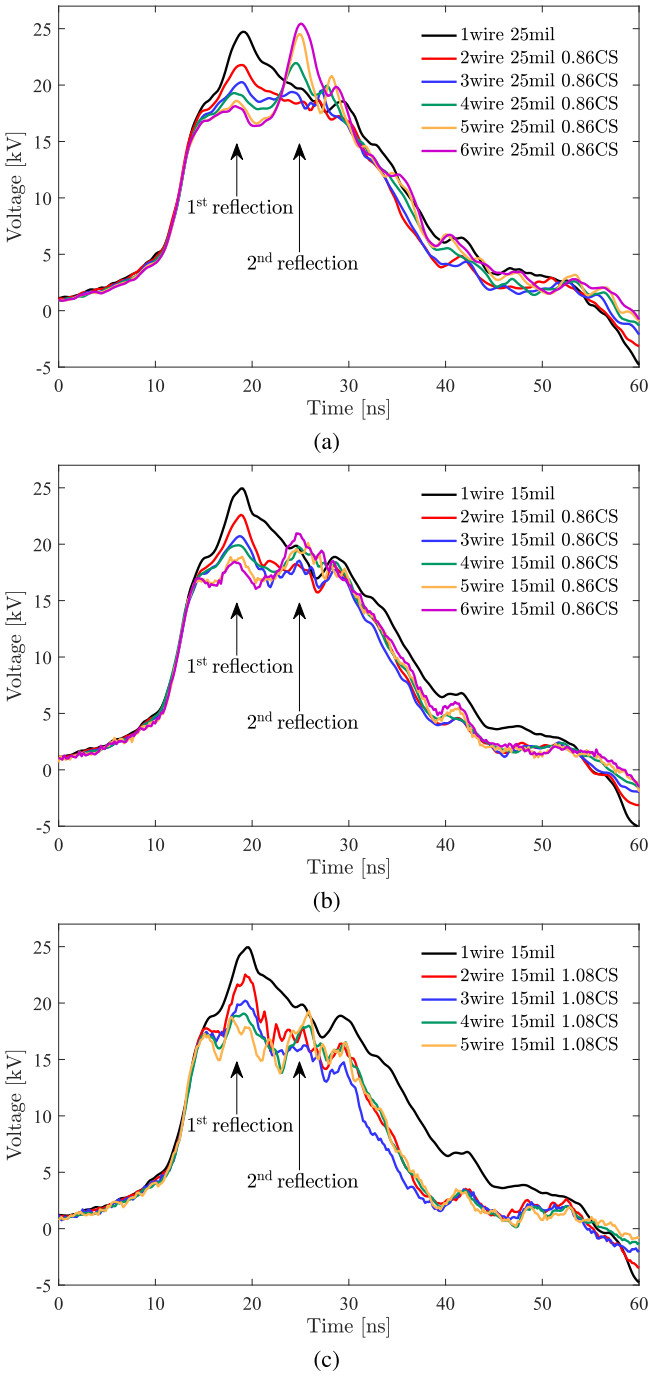

Fig. 12. Voltage at the sensor position as a function of different wire geometries, where wire diameter, cross section, and number of wires are varied. The voltage was measured at the D-dot sensor position for the same experimental settings as in Fig. 11.

D. Effect of Cross Section

In Fig. 12(c) the cross section is increased from 0.86 to 1.08 in and the second reflection is almost gone for all values of N_{w}. This is the result of the increased electric field at larger cross sections (the wires are closer to the reactor wall). Fig. 14 shows additional results on reactor efficiency, ozone yields, and system efficiencies for different cross sections. Now the reactor efficiency is not only boosted by the higher electric

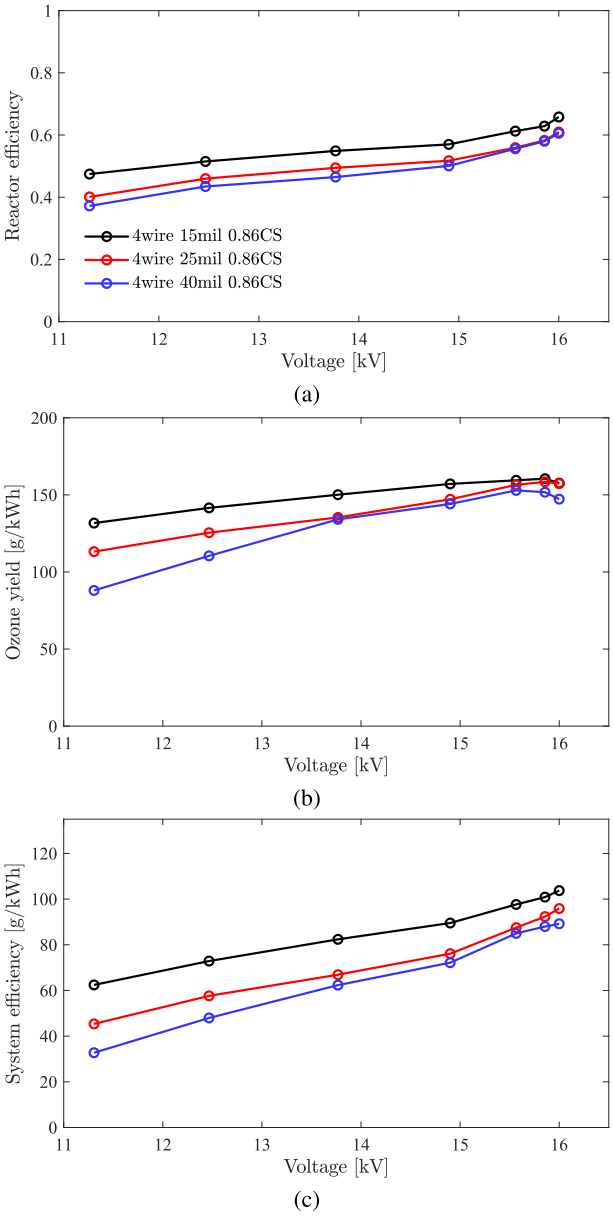

Fig. 13. (a) Reactor efficiency, (b) ozone yield, and (c) system efficiency as a function of the pulse voltage and the wire diameter used in the multiple-wire electrode assembly. The electrodes were 4-wire electrode assemblies with a 0.86-in cross section. The gas flow was 5 slm and the pulse repetition rate 50 Hz.

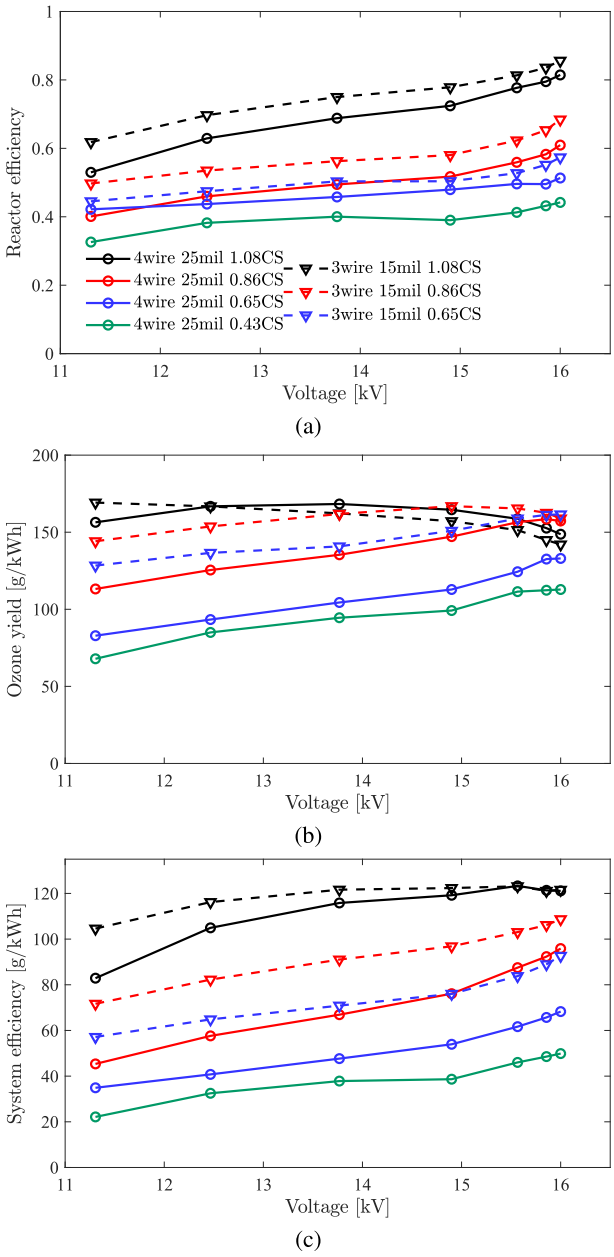

Fig. 14. (a) Reactor efficiency, (b) ozone yield, and (c) system efficiency as a function of the pulse voltage and the cross section used in the multiple-wire electrode assembly. The gas flow was 5 slm and the pulse repetition rate 50 Hz.

field at larger cross sections but also the reactor impedance is much lower for the larger cross sections (e.g., 77.1 Ω at 1.08 in versus 118 Ω at 0.43 in for the 25-mil wire). As the smaller cross section also reduces the ozone yield (because of the lower electric field), the system efficiency is significantly higher for the largest cross section electrode assemblies.

It should be noted that with the largest cross section we used (1.08 in) and $N_w > 3$ we were operating close to the limit of the reactor at the highest voltages: if the voltage was increased any further, spark discharges occurred in the reactor. The decrease in the ozone yield in Fig. 14(b) is also an indication of this. For instance, for the 6-wire electrode assembly in the results of Fig. 11 spark discharges occurred at the highest voltage setting.

E. Extruded Electrodes

Fig. 15 shows results on reactor efficiency, ozone yields and system efficiency for different electrode shapes. Here, we compare a 4-wire electrode assembly (of two different cross sections) to their extruded counterparts (see Fig. 8). As stated before, the reasoning behind using these electrodes is that they will potentially work as well as the 4-wire electrodes, but are much more sturdy and robust, which can be an advantage in real applications. Unfortunately, the results clearly show that these extruded electrodes reduce the reactor efficiency and system efficiency. It is likely (but this will have to be confirmed with electric field simulations) that the electric

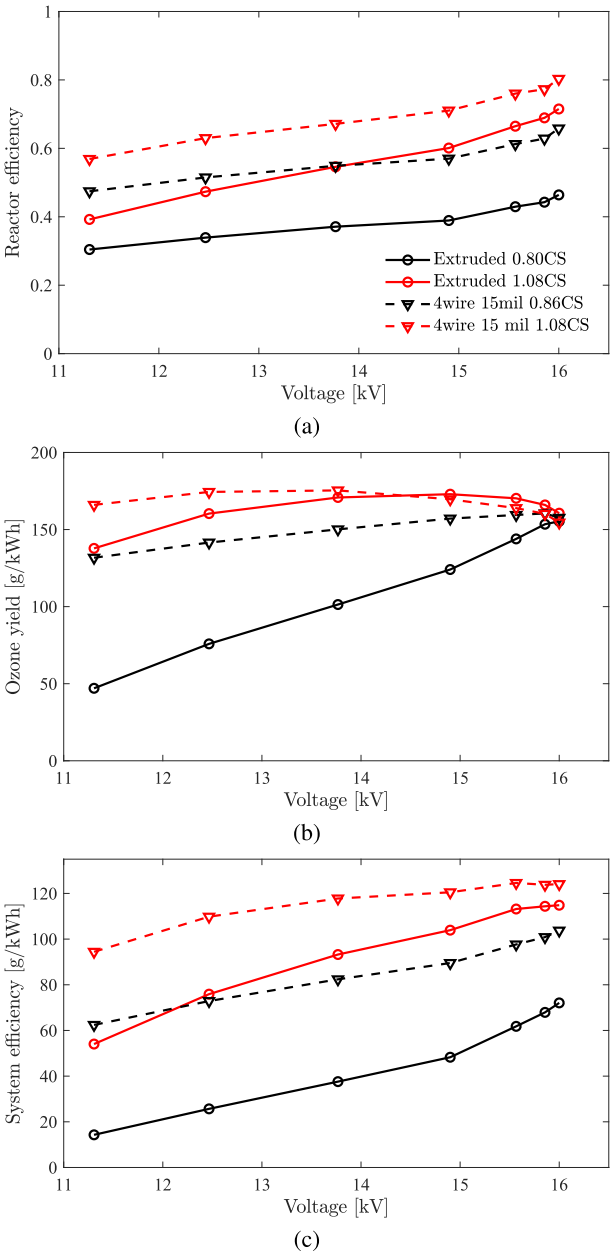

Fig. 15. (a) Reactor efficiency, (b) ozone yield, and (c) system efficiency as a function of the pulse voltage and the electrode shape (4-wire versus extruded electrodes). The gas flow was 5 slm and the pulse repetition rate 50 Hz.

field at the tips of the extruded electrodes were not as high as with the 4-wire electrodes, which would explain the poor performance.

F. Summary on System Efficiency and Voltage Stress

As a quick summary, Tables II and III show the reduced voltage stress and increased system efficiency, respectively, per electrode geometry as compared to a system with a standard 1-wire 15-mil electrode. The maximum achievable result is a very significant 29%–31% reduction on the voltage stress and a 95%–98% increase of the system efficiency when using a 4-wire or 5-wire electrode geometry at a cross section that is half the reactor diameter.

TABLE II

REDUCED VOLTAGE STRESS (AT 16-kV PULSE VOLTAGE) FOR THE DIFFERENT ELECTRODE GEOMETRIES AS COMPARED TO A STANDARD 1-WIRE 15-mil ELECTRODE

N	25mil 0.86CS	15mil 0.86CS	15mil 1.08CS
2	15%	10%	21%
3	23%	20%	23%
4	14%	25%	**31**%
5	2%	24%	29%
6	-2%	19%	

TABLE III

INCREASED SYSTEM EFFICIENCY (AT 16-kV PULSE VOLTAGE) FOR THE DIFFERENT ELECTRODE GEOMETRIES AS COMPARED TO A STANDARD 1-WIRE 15-mil ELECTRODE

N	25mil 0.86CS	15mil 0.86CS	15mil 1.08CS
2	51%	58%	78%
3	65%	71%	91%
4	50%	63%	95%
5	34%	72%	**98**%
6	13%	65%	

On a final note, we mention that even though there does not appear to be a discharge in the center of the multiple-wire electrode assemblies (see also Fig. 9) this has no significant effect on the efficiency of ozone generation in the system that we used in this study. In a real-world example where we used the system for diesel exhaust treatment, there also appeared to be no effect of this region without a discharge; also there the multiple-wire electrode outperformed the single-wire electrode significantly (see also the final note at the end of this article).

VI. SUMMARY, CONCLUSION, AND FUTURE WORK

In this article, we presented a study on boosting the energy efficiency of nanosecond pulsed corona plasma system by using a special type of plasma reactor: the multiple-wire plasma reactor. The basic principle of such a reactor is that it has a lower transmission-line impedance than a normal wire-cylinder reactor while at the same time still producing the required high electric fields necessary for plasma generation. The lower impedance of the reactor results in a smaller impedance mismatch between the high-voltage pulse source and the reactor, thereby minimizing pulse reflections on the source-reactor interface, increasing the energy efficiency of the system. We first calculated the impedance of the multiple-wire reactor and found a general expression that can be used to calculate this impedance (verified by numerical calculations). Then we assessed both the electrical energy efficiency as well as the chemical efficiency of the plasma by measuring electrical energies and ozone concentrations generated by the plasma for a range of multiple-wire plasma reactor parameters. We show that with the multiple-wire reactor we can almost double the energy efficiency of the reactor (from 45% to 85%), reduce the voltage stress in the system by 29%–31% and increase the system efficiency by 95%–98% when using a multiple-wire electrode geometry (as compared to a single-wire system). Also, from the results it seems that while the

lower impedance of the multiple-wire reactor certainly plays a role, the electric field generated by the multiple-wire reactor appears to have a more significant role in the increased reactor efficiency.

Finally in a future paper, we will describe a practical application example where we used the multiple-wire electrode geometry to boost the efficiency of a multi-kW pulsed corona system that we used for diesel exhaust remediation. In that system, we used two plasma reactors in parallel to decrease the total transmission-line impedance of the plasma reactor system even more and achieved reactor efficiencies of over 0.85 (85%).

REFERENCES

[1] H.-H. Kim, "Nonthermal plasma processing for air-pollution control: A historical review, current issues, and future prospects," *Plasma Process. Polym.*, vol. 1, no. 2, pp. 91–110, 2004.

[2] S. Samukawa *et al.*, "The 2012 plasma roadmap," *J. Phys. D: Appl. Phys.*, vol. 45, no. 25, 2012, Art. no. 253001.

[3] I. Adamovich *et al.*, "The 2017 plasma roadmap: Low temperature plasma science and technology," *J. Phys. D: Appl. Phys.*, vol. 50, Aug. 2017, Art. no. 323001.

[4] A. Fridman, A. Chirokov, and A. Gutsol, "Non-thermal atmospheric pressure discharges," *J. Phys. D: Appl. Phys.*, vol. 38, no. 2, p. R1, 2005.

[5] F. J. C. M. Beckers, W. F. L. M. Hoeben, T. Huiskamp, A. J. M. Pemen, and E. J. M. van Heesch, "Pulsed corona demonstrator for semi-industrial scale air purification," *IEEE Trans. Plasma Sci.*, vol. 41, no. 10, pp. 2920–2925, Oct. 2013.

[6] Y. Wu, J. Li, N. Wang, and G. Li, "Industrial experiments on desulfurization of flue gases by pulsed corona induced plasma chemical process," *J. Electrostatics*, vol. 57, no. 3, pp. 233–241, 2003.

[7] Y. S. Mok and S. W. Ham, "Conversion of NO to NO_2 in air by a pulsed corona discharge process," *Chem. Eng. Sci.*, vol. 53, no. 9, pp. 1667–1678, 1998.

[8] E. H. W. M. Smulders, B. E. J. M. van Heesch, and S. S. V. B. van Paasen, "Pulsed power corona discharges for air pollution control," *IEEE Trans. Plasma Sci.*, vol. 26, no. 5, pp. 1476–1484, Oct. 1998.

[9] Y.-H. Lee *et al.*, "Application of pulsed corona induced plasma chemical process to an industrial incinerator," *Environ. Sci. Technol.*, vol. 37, no. 11, pp. 2563–2567, 2003.

[10] E. J. M. van Heesch, G. J. J. Winands, and A. J. M. Pemen, "Evaluation of pulsed streamer corona experiments to determine the O^* radical yield," *J. Phys. D: Appl. Phys.*, vol. 41, no. 23, 2008, Art. no. 234015.

[11] R. Ono, Y. Nakagawa, and T. Oda, "Effect of pulse width on the production of radicals and excited species in a pulsed positive corona discharge," *J. Phys. D: Appl. Phys.*, vol. 44, no. 48, 2011, Art. no. 485201.

[12] T. Matsumoto, D. Wang, T. Namihira, and H. Akiyama, "Energy efficiency improvement of nitric oxide treatment using nanosecond pulsed discharge," *IEEE Trans. Plasma Sci.*, vol. 38, no. 10, pp. 2639–2643, Oct. 2010.

[13] W. Douyan, T. Namihira, and H. Akiyama, "Recent progress of nanoseconds pulsed discharge and its applications," *J. Adv. Oxidation Technol.*, vol. 14, no. 1, pp. 131–137, Jan. 2011.

[14] T. Huiskamp, W. F. L. M. Hoeben, F. J. C. M. Beckers, E. J. M. van Heesch, and A. J. M. Pemen, "(Sub)nanosecond transient plasma for atmospheric plasma processing experiments: Application to ozone generation and NO removal," *J. Phys. D: Appl. Phys.*, vol. 50, no. 40, 2017, Art. no. 405201.

[15] G. J. J. Winands, Z. Liu, E. J. M. van Heesch, A. J. M. Pemen, and K. Yan, "Matching a pulsed-power modulator to a streamer plasma reactor," *IEEE Trans. Plasma Sci.*, vol. 36, no. 1, pp. 243–252, Feb. 2008.

[16] T. Matsumoto, D. Wang, T. Namihira, and H. Akiyama, "Improvement of impedance matching between ns pulse generator and discharge reactor," in *Proc. IET Eur. Conf. Eur. Pulsed Power*, 2009, pp. 1–4.

[17] H. Ma and Y. Qiu, "A study of ozone synthesis in coaxial cylinder pulse streamer corona discharge reactors," *Ozone, Sci. Eng.*, vol. 25, no. 2, pp. 127–135, 2003.

[18] S.-H. Kim, M. Ehsani, Y.-H. Kim, and C.-H. Choi, "Design and implementation of the plasma reactor for pulsed power system," *IEEE Trans. Dielectr. Electr. Insul.*, vol. 20, no. 4, pp. 1117–1122, Aug. 2013.

[19] T. Huiskamp, F. J. C. M. Beckers, W. F. L. M. Hoeben, E. J. M. van Heesch, and A. J. M. Pemen, "Matching a (sub)nanosecond pulse source to a corona plasma reactor," *Plasma Sources Sci. Technol.*, vol. 25, no. 5, 2016, Art. no. 054006.

[20] K. Yan, E. J. M. van Heesch, A. J. M. Pemen, and P. A. H. J. Huijbrechts, "From chemical kinetics to streamer corona reactor and voltage pulse generator," *Plasma Chem. Plasma Process.*, vol. 21, no. 1, pp. 107–137, 2001.

[21] T. M. P. Briels, J. Kos, E. M. van Veldhuizen, and U. Ebert, "Circuit dependence of the diameter of pulsed positive streamers in air," *J. Phys. D: Appl. Phys.*, vol. 39, no. 24, p. 5201, 2006.

[22] T. M. P. Briels, J. Kos, G. J. J. Winands, E. M. van Veldhuizen, and U. Ebert, "Positive and negative streamers in ambient air: Measuring diameter, velocity and dissipated energy," *J. Phys. D: Appl. Phys.*, vol. 41, no. 23, Dec. 2008, Art. no. 234004.

[23] I. Kornev, F. Saprykin, and S. Preis, "Stability and energy efficiency of pulsed corona discharge in treatment of dispersed high-conductivity aqueous solutions," *J. Electrostatics*, vol. 89, pp. 42–50, Oct. 2017.

[24] A. J. M. Pemen, I. V. Grekhov, E. J. M. van Heesch, K. Yan, S. A. Nair, and S. V. Korotkov, "Pulsed corona generation using a diode-based pulsed power generator," *Rev. Sci. Instrum.*, vol. 74, no. 10, pp. 4361–4365, 2003.

[25] T. Huiskamp, N. Takamura, T. Namihira, and A. J. M. Pemen, "Matching a nanosecond pulse source to a streamer corona plasma reactor with a DC bias," *IEEE Trans. Plasma Sci.*, vol. 43, no. 2, pp. 617–624, Feb. 2015.

[26] T. Huiskamp, A. J. M. Pemen, W. F. L. M. Hoeben, F. J. C. M. Beckers, and E. J. M. van Heesch, "Temperature and pressure effects on positive streamers in air," *J. Phys. D: Appl. Phys.*, vol. 46, no. 16, pp. 165202–165210, 2013.

[27] S. Pancheshnyi, M. Nudnova, and A. Starikovskii, "Development of a cathode-directed streamer discharge in air at different pressures: Experiment and comparison with direct numerical simulation," *Phys. Rev. E, Stat. Phys. Plasmas Fluids Relat. Interdiscip. Top.*, vol. 71, Jan. 2005, Art. no. 016407.

[28] R. Ono and T. Kamakura, "Pulsed positive streamer discharges in air at high temperatures," *Plasma Sources Sci. Technol.*, vol. 25, Jul. 2016, Art. no. 044007.

[29] R. Ono and Y. Ishikawa, "The effect of temperature on pulsed positive streamer discharges in air over the range 292 K–1438 K," *J. Phys. D: Appl. Phys.*, vol. 51, Apr. 2018, Art. no. 185204.

[30] D. Z. Pai, D. A. Lacoste, and C. O. Laux, "Transitions between corona, glow, and spark regimes of nanosecond repetitively pulsed discharges in air at atmospheric pressure," *J. Appl. Phys.*, vol. 107, no. 9, 2010, Art. no. 093303.

[31] A. Mizuno *et al.*, "Non-thermal plasma applications at very low temperature," *Combustion Sci. Technol.*, vol. 133, nos. 1–3, pp. 49–63, 1998.

[32] S. A. Nair *et al.*, "A high-temperature pulsed corona plasma system for fuel gas cleaning," *J. Electrostatics*, vol. 61, no. 2, pp. 117–127, 2004.

[33] K. Yoshinaga, S. Okada, D. Wang, T. Namihira, S. Katsuki, and H. Akiyama, "Effect of polarity and rise time of applied pulsed voltage on streamer discharge phenomena," *Acta Phys. Pol. A*, vol. 115, no. 6, p. 1050, 2009.

[34] T. Huiskamp, "Nanosecond pulsed streamer discharges part I: Generation, source-plasma interaction and energy-efficiency optimization," *Plasma Sources Sci. Technol.*, vol. 28, 2019, doi: 10.1088/1361-6595/ab53c5.

[35] H. Kaden, *Wirbelströme und Schirmung in der Nachrichtentechnik*. Berlin, Germany: Springer, 1959.

[36] *OpenFOAM*. Accessed: Aug. 1, 2019. [Online]. Available: https://openfoam.org/

[37] J. D. Jackson, *Classical Electrodynamics*. Hoboken, NJ, USA: Wiley, 1975.

[38] Transient Plasma Systems. Accessed: Aug. 1, 2019. [Online]. Available: http://www.transientplasmasystems.com

[39] T. Huiskamp, F. J. C. M. Beckers, E. J. M. van Heesch, and A. J. M. Pemen, "B-dot and D-dot sensors for (sub)nanosecond high-voltage and high-current pulse measurements," *IEEE Sensors J.*, vol. 16, no. 10, pp. 3792–3801, May 2016.

[40] B. M. Novac *et al.*, "Theoretical and experimental studies of off-the-shelf V-dot probes," *IEEE Trans. Plasma Sci.*, vol. 46, no. 8, pp. 2985–2992, Aug. 2018.

[41] F. J. C. M. Beckers, "Pulsed power driven industrial plasma processing," Ph.D. dissertation, Dept. Elect. Eng., Eindhoven Univ. Technol., Eindhoven, The Netherlands, 2015. [Online]. Available: http://repository.tue.nl/801599

[42] D. Braun, U. Küchler, and G. Pietsch, "Behaviour of NO_x in air-fed ozonizers," *Pure Appl. Chem.*, vol. 60, no. 5, pp. 741–746, 1988.
[43] B. Eliasson and U. Kogelschatz, "Modeling and applications of silent discharge plasmas," *IEEE Trans. Plasma Sci.*, vol. 19, no. 2, pp. 309–323, Apr. 1991.
[44] J. Kitayama and M. Kuzumoto, "Theoretical and experimental study on ozone generation characteristics of an oxygen-fed ozone generator in silent discharge," *J. Phys. D: Appl. Phys.*, vol. 30, no. 17, p. 2453, 1997.

T. Huiskamp (M'16) was born in Den Dolder, The Netherlands, in 1985. He received the M.Sc. degree (Hons.) and the Ph.D. degree (Hons.) in electrical engineering from the Eindhoven University of Technology (TU/e), Eindhoven, The Netherlands, in 2011 and 2015, respectively.

As a Ph.D. Researcher, he worked on nanosecond pulsed power induced corona plasmas with the Electrical Energy Systems Group, Eindhoven University of Technology, where he currently works as an Assistant Professor. As a Visiting Researcher, he worked at the Kumamoto University, Kumamoto, Japan, the University of Southern California, Los Angeles, CA, USA, and the Leibniz Institute for Plasma Science and Technology (INP), Greifswald, Germany. His main area of expertise is flexible, adjustable parameter (sub) nanosecond pulse source development and their application to transient plasmas for air purification and plasma-activated water generation applications.

S. Subramanian was born in Mumbai, India, in 1991. He received the M.S. degree in electrical engineering from the University of Southern California (USC), Los Angeles, CA, USA, in 2016.

During his time at the USC Pulsed Power Research Group, he worked on diesel pollutant abatement using nanosecond pulsed power. He continues to work as a Research Assistant with the USC Pulsed Power Research Group, while pursuing the second M.S. degree in data analytics. He specializes in interfacing pulsed power sources to diesel pollutant abatement applications, fast rising current and voltage pulse measurements, and pulsed power sources.

V. Gururajan was born in Tamil Nadu, India. He received the master's and Ph.D. degrees in aerospace and mechanical engineering from the University of Southern California, Los Angeles, CA, USA, in 2011 and 2016, respectively, his Ph.D. focus was on high-fidelity numerical simulations of canonical combustion experiments and the study of low-temperature plasma kinetics.

He currently works as a Post-Doctoral Appointee with the Argonne National Laboratory, Lemont, IL, USA, where he undertakes the numerical study of streamer discharges in ignition systems.

W. P. Schroeder received research support from the TCC Group through the University of Southern California (USC), Los Angeles, CA, USA. He continues to serve in an advisory capacity as a paid consultant for the TCC Group.

C. A. Schroeder received the B.S. degree in chemistry from Missouri Western State University, Saint Joseph, MO, USA, in 2004, and the Ph.D. degree from the University of Southern California, Los Angeles, CA, USA, in 2012, under the supervision of Prof. S. Bradforth.

Following a five year tenure working in the field of air quality regulation as a Senior Scientist with the South Coast Air Quality Management District, she returned to the University of Southern California to join the Ming Hsieh Department of Electrical Engineering-Electrophysics as a Senior Scientist. Her current research interest lie at the intersection of plasma assisted remediation of combustion process pollutants and analytical and regulatory testing methodology as it applies to air quality regulation policy and compliance.

M. A. Gundersen (M'74–SM'83–F'91–LF'08) is currently the Lloyd Hunt Professor of electrical power engineering and a Professor of electrical engineering, physics, and materials science with the University of Southern California, Los Angeles, CA, USA. His current research interests include nanosecond pulsed power, engine ignition, and combustion technologies for emissions reduction and improved efficiencies in a range of engines.

Dr. Gundersen is a fellow of the Optical Society of America. He received the Germeshausen Award at the IEEE Power Modulator Conference, the Sol Schneider Award at the 2010 IEEE Power Modulator and High Voltage Conference, the 2015 USC Associates Award for Creativity in Research and Innovation, the 2018 American Institute of Aeronautics and Astronautics Plasmadynamics and Lasers Award, and the 2018 Bioelectromagnetics Society Award for the most influential article for 2012–2016. He has chaired and organized technical meetings, including the 1980 OSA Topical Meeting on IR Lasers, the 1989 NATO Advance Research Workshop, the Power Modulator Symposium in 1990 and 1998, and the Workshops at the American Film Institute for the purpose of improving science portrayals in film. He served as the Chair for the Ming Hsieh Department of Electrical Engineering-Electrophysics, from 1998 to 2003, where he has published in laser, solid state, pulsed power, combustion, and other areas of research.

S. B. Cronin received the B.S. degree in physics from New York University, New York, NY, USA, in 1996, and the Ph.D. degree in physics from the Massachusetts Institute of Technology, Cambridge, MA, USA, in 2002, under the supervision of Prof. M. Dresselhaus.

He joined the Ming Hsieh Department of Electrical Engineering-Electrophysics, University of Southern California, Los Angeles, CA, USA, in August 2005. He holds joint appointments with the Departments of Chemistry and Physics. He has over 150 technical publications in peer-reviewed journals and holds five patents. His current research interest focuses on a broad range of interrelated topics in physics, chemistry, electrical engineering, and materials science.

Dr. Cronin received several awards, including the National Science Foundation's Faculty Early Career Development (CAREER) Award and the U.S. Air Force Office of Scientific Research (AFOSR) Young Investigator Award. He was later promoted to the Gordon S. Marshall Early Career Chair in engineering from 2010 until becoming a Full Professor in 2016.